Precise multi-image pointing (MIP) applied on convergence close-range photogrammetry images

Farid Esmaeili
Department of Surveying Engineering, Zanjan Branch, Islamic Azad University, Zanjan, Iran
Hamid Ebadi
Department of Photogrammetry and Remote Sensing, Faculty of Geodesy and Geomatics Engineering, K.N. Toosi University of Technology, Tehran, Iran
Mohammad Saadatseresht
Department of Photogrammetry and Remote Sensing, School of Surveying and Geospatial Engineering, College of Engineering, University of Tehran, Tehran, Iran, and
Farzin Kalantary
Department of Geotechnical Engineering, Faculty of Civil Engineering, K.N. Toosi University of Technology, Tehran, Iran

Abstract

Purpose – Displacement measurement in large-scale structures (such as excavation walls) is one of the most important applications of close-range photogrammetry, in which achieving high precision requires extracting and accurately matching local features from convergent images. The purpose of this study is to introduce a new multi-image pointing (MIP) algorithm is introduced based on the characteristics of the geometric model generated from the initial matching. This self-adaptive algorithm is used to correct and improve the accuracy of the extracted positions from local features in the convergent images.

Design/methodology/approach – In this paper, the new MIP algorithm based on the geometric characteristics of the model generated from the initial matching was introduced, which in a self-adaptive way corrected the extracted image coordinates. The unique characteristics of this proposed algorithm were that the position correction was accomplished with the help of continuous interaction between the 3D model coordinates and the image coordinates and that it had the least dependency on the geometric and radiometric nature of the images. After the initial feature extraction and implementation of the MIP algorithm, the image coordinates were ready for use in the displacement measurement process. The combined photogrammetry displacement adjustment (CPDA) algorithm was used for displacement measurement between two epochs. Micro-geodesy, target-based photogrammetry and the proposed MIP methods were used in a displacement measurement project for an excavation wall in the Velenjak area in Tehran, Iran, to evaluate the proposed algorithm performance. According to the results, the measurement accuracy of the point geo-coordinates of 8 mm and the displacement accuracy of 13 mm could be achieved using the MIP algorithm. In addition to the micro-geodesy method, the accuracy of the results was matched by the cracks created behind the project's wall. Given the maximum allowable displacement limit of 4 cm in this project, the use of the MIP algorithm produced the required accuracy to determine the critical displacement in the project.

Findings – Evaluation of the results demonstrated that the accuracy of 8 mm in determining the position of the points on the feature and the accuracy of 13 mm in the displacement measurement of the excavation walls could be achieved using precise positioning of local features on images using the MIP algorithm.The proposed algorithm can be used in all applications that need to achieve high accuracy in determining the 3D coordinates of local features in close-range photogrammetry.

Originality/value – Some advantages of the proposed MIP photogrammetry algorithm, including the ease of obtaining observations and using local features on the structure in the images rather than installing the artificial targets, make it possible to effectively replace micro-geodesy and instrumentation methods. In addition, the proposed MIP method is superior to the target-based photogrammetric method because it does not need artificial target installation and protection. Moreover, in each photogrammetric application that needs to determine the exact point coordinates on the feature, the proposed algorithm can be very effective in providing the possibility to achieve the required accuracy according to the desired objectives.

Keywords Close-range photogrammetry, Local features extraction, Soil nail wall, Deformation measurement, Camera calibration, Network design

Paper type Research paper

The current issue and full text archive of this journal is available on Emerald Insight at: **https://www.emerald.com/insight/0260-2288.htm**

Sensor Review
40/3 (2020) 311–328
 [ISSN 0260-2288]
[DOI 10.1108/SR-12-2019-0314]

The authors would like to appreciate Iran National Science Foundation for supporting this research. Also, the authors would like to thank Sarang Seyrafiyan for his great efforts in providing the data-collecting situations as well as Sepehr Seyedashrafi and Vahid Alimoradi for their kind help during the project.

Received 13 December 2019
Revised 23 February 2020
Accepted 18 March 2020

1. Introduction

Excavation in the expensive urban lands, to construct underground structures for optimal use of property even up to a depth of more than 30 m, is quite popular. Soil nailing and anchorage are some of the most common ways to stabilize the excavation walls. The step-by-step bracing of the excavation wall using the nailing method has some advantages including higher speed, lower costs and a higher range of reliability compared to other retaining structures. Because of the sensitivity of the excavation projects, displacement measurement and monitoring of the wall behavior during excavation or afterward are among the main components of such projects. Mostly, two methods, namely, micro-geodesy and instrumentation (such as strain gauges), are applied for the displacement measurement of the excavation walls. These methods have their own limitations including high cost, time-consuming observations, limited accuracy, low flexibility, high dependency on project conditions and the need for specialized personnel to name but a few. These limitations adversely affect the control process of the project from a geotechnical point of view. Close-range photogrammetry has unique properties as an accurate measurement tool in large-scale structures. The possibility of fast acquisition of observations, the potential to achieve the accuracies in the order of sub-millimeters, the possibility of texture mapping and the real modeling of the feature, obtaining archival images and converting images to the map for the future possible use, high density of the acquired cloud points from the feature, lower cost, high diversity in measurable feature dimensions, real-time measurements and many other advantages have led to a drastic increase in the use of photogrammetric measurement techniques in the field of large-scale displacement measurements.

In the authors' previous research, Esmaeili *et al.* (2013) proposed the close-range photogrammetry method in 2013 for the measurement of the displacement of excavation walls. It was demonstrated in this study that a displacement measurement accuracy of 8 mm can be obtained using the proposed combined photogrammetry displacement adjustment (CPDA) [1] method and installing photogrammetric targets on the structure (Esmaeili *et al.*, 2013, 2019a, 2019b). Li *et al.* (2015) measured unsaturated soil deformations during triaxial testing using a photogrammetry-based method. Xiao *et al.* (2010) measured the displacement of a transmission tower under different loadings with the close-range photogrammetry method. In this research, to determine the corresponding targets that represented displacement at a point, a simple innovative method based on the search for the closest neighbor after coordinate confirmation was used. Jiang and Jauregui (2010) measured the deformation in a steel road bridge as a result of loading using close-range photogrammetry. They proposed the refined distance constraint (RDC) [2] method for controlling the close-range photogrammetry network and used double-sided targets for this purpose (Jiang and Jauregui, 2010; Jiang, 2005). Feng *et al.* (2016) measured surface changes in a scaled-down landslide model using high-speed stereo image sequences. Ozbek *et al.* (2010) measured the vibration frequency of a rotating wind turbine blade using a real-time photogrammetry system. Alba *et al.* (2010) presented the development and the results of a fast method for displacement measurement based on digital images, which allows a deformation analysis along the cross-sections of a tunnel via vision metrology (Alba *et al.*, 2010; Scaioni *et al.*, 2014). Fraser *et al.* (2005) measured the changes in the Hobart radio telescope surface as a result of an antenna angle change in three modes with respect to the vector model available from its surface with the close-range photogrammetry method. They achieved the predetermined precisions in the measurements by introducing the notion of hyper-redundancy (Fraser *et al.*, 2005). Fraser *et al.* (2003) measured the displacement of the suspended part of the North Atrium structure at Federation Square in Melbourne, Australia as a result of jacking and glass installation using the close-range photogrammetry technique based on coded targets with automatic measurements (Fraser *et al.*, 2003; Miller, 2009). Lee and Al-Mahaidi (2008) used the close-range photogrammetry method to investigate the load-deformations characteristics of reinforced concrete T-beams strengthened with carbon-fiber-reinforced polymer plates (Lee and Al-Mahaidi, 2008; Miller, 2009). Fraser (1999) used close-range photogrammetry to monitor the behavior of an ore crusher device in a gold mine in the specification of the changes in the distance between the rotor and stator parts of the motor as a result of changes in the voltage of the device (Fraser, 2001; Miller, 2009). Fraser and Riedel (2000) reported multi-epoch deformation monitoring of a series of super-hot steel beams with digital close-range photogrammetry. The deformations resulted from the cooling of the super-hot steel beams, where the close-range photogrammetry method proved effective for this purpose (Fraser and Riedel, 2000; Miller, 2009). Li and King (2002) used the close-range photogrammetry method to monitor the deformation in the colonnade of the Star Ferry Cultural and Arts Center structure in Hong Kong as a result of underground canal excavation (Li and King, 2002). Cerminaro (2014) used close-range photogrammetry to improve proactive assessment of retaining walls along transportation corridors. He made use of dense surface measurement and surface matching to measure displacement (Cerminaro, 2014). Valença and Júlio (2017) developed a photogrammetry based method to monitoring load tests on reinforced concrete framed structures, with or without masonry wall infill (Valença and Júlio, 2017). Sundla *et al.* (2015) proposed an easy-to-use approach using cubic spline interpolation for providing initial estimations for digital image correlation grid point locations and rotations on objects with major deflection (Sundla *et al.*, 2015). Scaioni *et al.* (2015) organized image-based deformation measurement applications into three main categories:

1. photogrammetric coded-target measurements;
2. surface-point tracking to reconstruct dense displacement fields; and
3. comparison of surfaces obtained from dense image matching (Scaioni *et al.*, 2015).

Oats *et al.* (2017) evaluated the failure modes of a 2.43 m × 2.43 m retaining wall model using three-dimensional (3D) photogrammetry as a cost-effective quantitative alternative for retaining wall monitoring. Luo *et al.* (2017) measured the effect of pressure on large inflatable structures using close-range photogrammetry. They measured the displacements resulting from pressure change on uneven and irregular surfaces by combining the digital photogrammetry

and Delaunay triangulation methods (Luo *et al.*, 2017). Tsvetkov *et al.* (2017) used close-range photogrammetry for deformation monitoring of load-bearing reinforced concrete beams. They used internet protocol cameras, which transfer images to the server with wireless technologies (Tsvetkov *et al.*, 2017). Barazzetti and Scaioni (2010) presented the development and implementation of three image-based methods used to detect and measure the displacements of a vast number of points in the case of laboratory testing on construction materials. They made a comparison between the modes of using artificial targets and dense marketing without using targets for measuring the displacement of a concrete beam under pressure. In both modes, it has been possible to dynamically measure the displacement of the structure with the required precisions (Barazzetti and Scaioni, 2010). Table 1 shows a comparison between different parameters and features in some of the latest research conducted on displacement measurement of large-scale structures with the close-range photogrammetry method.

According to Table 1, in all of the investigated projects, concerning to the project structure, close-range photogrammetry was able to achieve the required accuracy in displacement measurements (Esmaeili *et al.*, 2019a, 2019b). The designing flexibility of the close-range photogrammetric systems to achieve the desired precision makes it possible to create special constraints and additional observations to increase the accuracy of measurement in project conditions. There are some unique advantages for photogrammetric methods that none of the other methods has such capabilities. Some of these advantages are listed as follows: there is no need for direct contact to the structure during the data acquisition, it allows rapid preparation of feature observations, it gives instant access to the results by automating the algorithms, it has the ability to record instantaneous observations of moving features and it gives the possibility of archiving observations for future processing, if needed.

Projects regarding displacement measurement of large-scale structures that apply photogrammetric methods include four stages:

1 a network design and network control system that determines the camera positions, camera type and settings, the base coordinate system and resolving the scale issue;
2 convergent imaging of the features;
3 calculating and extracting the 3D point coordinates on the feature for each epoch that includes the following steps:
   - feature extraction, which selects salient features in two images (reference image and input image), such as corners, blobs and regions
   - feature description, which generates feature attributes ("descriptors" to characterize and match them) using various image properties such as intensity, color, texture and edge
   - feature matching, which establishes the correspondence between the features in the two images using particular similarity measures of their descriptors and then uses a consistency check process to remove probable mismatches
   - calculating 3D coordinates of the matched points using the bundle adjustment method based on the collinearity equation
4 displacement calculation by comparing the point coordinates in two epochs in one coordinate system.

Because of the sensitivity of displacement projects in terms of achieving high precision, in all of the aforementioned studies, photogrammetric targets were used to extract accurate photo-observations. The retro-reflective photogrammetric targets, because of their specific geometric shape and high contrast in the image, make it possible to extract unique and similar points in convergent images from the features. Therefore, in the feature detection step, they lead to detailed extraction of photo-observations and increase measuring displacement accuracy. Also, the use of coded targets allows for automatic matching of targets with the help of template matching algorithms.

Characteristics or image patterns that are uniquely distinguishable from their neighbors are called "local features" (Tuytelaars and Mikolajczyk, 2008), and determination of the corresponding local features or pixels in various images from an object is called "matching." Generally, in extraction algorithms, the following should be considered: local features (corners, edges, blobs and regions), characters with repeatability, distinctiveness/informativeness, locality, quantity, accuracy, efficiency, invariance and robustness. In most researches conducted in this area, these methods require the installation of artificial targets for the feature extraction stage. As stated, one of the main goals of using artificial targets in close-range photogrammetry projects is to increase the feature extraction accuracy. For example, knowing the target is circular, its center of gravity can be extracted as a local feature using a region-based method. Targets lead to potentially 5–10 times the point positioning accuracy of feature-based extraction/matching (i.e. 0.05–0.1 pixel versus 0.3–0.4 pixel); there is no ambiguity about the matching points, so point "tracking" is more straightforward, and the targeted approach affords a fully automatic deformation monitoring. One can achieve very good point correspondences between epochs if template matching is used.

However, the use of artificial targets in displacement measurement projects for the excavation wall has many limitations. In some projects, it is not possible to use artificial targets because of the project conditions. Shotcrete coverage of the target surface during the project, maintenance, the limited number of targets and the target installation difficulties are some obstacles in using artificial targets as a base point for the displacement measurements of the excavation walls by photogrammetry. However, in some of the conditions described in the following, local features cannot provide accuracy and robustness for features in the images as a photogrammetric target.

The results of local feature extraction algorithms depend on various parameters in the images. The convergence object images may have geometric or radiometric differences. In such cases, the local feature extraction algorithm exhibits different behavior in terms of its different characteristics, such as accuracy, efficiency and robustness. Parameters that may impede the image extraction and matching process include (Schmid and Mohr, 1997; Tuytelaars and Mikolajczyk, 2008) the following:

- *Geometric differences between images*: Convergent images taken from a feature may be geometrically different from

Table 1 Specifications of measuring displacement projects on a variety of large-scale structures by close-range photogrammetry

Research fellow	Measured structure	Measurement type	Targeting and imaging type	Utilized camera	Network control	Displacement measurement accuracy	Used software	Project special conditions
Esmaeili *et al.* (2019a, 2019b)	Supported excavation wall using nailing method	3D displacement without using photogrammetry targets	No use of targets/UAV photogrammetry imaging	Sony EXMOR 1/2.3″ – 4 K	Measuring displacement using the CPDA method and scale bars	Better than ±1 cm	Developed code in MATLAB	Photogrammetry network development using UAV imaging
Luo *et al.* (2017)	Large inflatable structures	Strain fields from a circular fabric film subjected to a bulge test	Retro-reflective targets and coded targets	INCA3	Measuring displacement with Delaunay triangulation and using finite element method EFM [3]	Approximately ±1 mm	V-STARS	Delaunay triangulation between targets
Cerminaro (2014)	Retaining wall between non-level highways	Displacement measurement of retaining wall between two epochs	Retro-reflective targets on the wall/pinhole camera model	Nikon D5100	Measuring displacement based on cloud point matching	Approximately ±5 mm	AgisoftPhotoscan Profession and Cloud Compare	Monitoring the retaining wall in separation joint
Scaioni *et al.* (2014)	Tunnel monitoring	Displacement measurement in the cross-section plane of the tunnel	Double-face photogrammetry targets/ convergence imaging	Nikon D80and Nikon D700	special targeted rods as scale bars	better than ±0.3 mm	iWitness	Using photogrammetric leveling for optical leveling of targets
Esmaeili *et al.* (2013)	Supported excavation wall using nailing method	3D displacement towards the excavation site	Retro-reflective targets on wall and out of excavation as control point – shooting with flash	Canon PowerShot SX130 IS	Measuring displacement using CPDA independent of external data	±7 mm	Australisand MATLAB	Monitoring between progressing excavation epochs
Xiao *et al.* (2010)	Transmission tower	Load–deformationmeasurement	Non-coded and coded retro-reflective targets – an external ring flash is adopted	CANON400D (SLR)	Using coded targets in stationary positions for epoch results match	±0.1 mm/m	3D optical deformation measurement system called XJTUSD is developed with VC++	Measuring displacement was performed in 10 epochs with different pressure changes
Jiang and Jauregui (2010)	Steel bridge	Bridge Deformation during loading	Retro-reflective targets on the body and tripod – shooting with a flash	Kodak DCS660 and Kodak Pro SLR/n	Using level targets RDC method	1 mm in *X* and *Y* directions and ±2 mm in the *Z* direction	PhotoModeler	Monitoring between loading epochs
Ozbek *et al.* (2010)	Wind turbine	Deformation because of wind on turbine	Retro-reflective targets on blades and column – shooting with flash	Four CCD cameras	Using Markers	±25 mm	GOM PONTOS system	Real-time monitoring

one another. The differences can result from differences in the scale of an image, small imaging angles between the optical axis direction and the feature, deformation of the feature because of changed imaging angle and view to the feature, the existence of concealed areas in an image that are exposed in another image and displacement caused by different heights and different perspectives in the images.

- *Presence of special conditions in the texture of the features in the image*: In some cases, features across the image exhibit repetitive and homogeneous textures (e.g. concreted or nailed excavation wall). Furthermore, positions of particular objects (e.g. buildings and trees) in front of the excavation walls create some sort of ambiguities in the anticipated texture in that area. Also, the presence of surfaces with a poor texture (e.g. wall of buildings or excavated surfaces) creates some ambiguities during the feature extraction process.
- *Radiometric changes in the overlapping images taken from the feature*: Radiometric changes such as shadow, luminous intensity, dust, the noises generated, because of the failure to properly adjust radiometric parameters of the imaging camera, and changes in the solar altitude angle can induce some changes in the images and present some challenges in extracting the same features from different images.

Among the aforementioned parameters, changing the image perspective leads to geometric changes in the overlapping images from the feature. These changes are one of the most important factors influencing the accuracy of local feature positioning in the displacement measurement of large-scale structures using close-range convergent images. In other words, because for the accuracy of the imaging network, it is necessary to take images from different angles with respect to the feature in the form of a convergent network, the features will show perspective differences in the images. These perspective differences result in a situation where similar features in covered images taken from different angles are not extracted with adequate accuracy. As a result, low-accurate image coordinates keep us from achieving high accuracy in displacement evaluation using these extracted features.

Of course, other parameters such as radiometric changes, displacement because of differences in elevation, shadow and texture issues in the image contribute to this problem. Because artificial targets resolve these problems to some extent, they are used in most displacement measurement projects that apply close-range photogrammetric techniques. However, as stated, the use of these targets has many limitations such that sometimes it is impossible to use the effective close-range photogrammetric techniques. When a property of local feature and its extraction algorithm is critical for an application (such as positioning accuracy), the applicability of the photogrammetric technique to those applications faces some difficulties (for example, the displacement measurement for structures on which targets cannot be installed). In other words, if a feature with proper position accuracy cannot be extracted in all convergent images, close-range photogrammetry can hardly be used to evaluate the displacement of a feature on which no target can be installed. This is not just about displacement measurement, but for any applications that require accurate feature measurements utilizing photogrammetric methods, accurate feature extraction from the images is of crucial importance. In this paper, a new self-adaptive algorithm, known as multi-image pointing (MIP), is introduced using a set of convergent images from the feature to increase the local feature extraction accuracy. In the following, the proposed algorithm is explained, then the application of the algorithm in some case studies is presented, and, finally, the results will be discussed.

2. Methodology of the proposed method

In this section, a new strategy and algorithm are proposed to increase the local feature extractor accuracy using a set of convergent images taken from the feature by means of determining the local feature 3D coordinates. This algorithm was used in measuring displacement in excavation walls. The main steps in the implementation of the algorithm components and its main part and the MIP algorithm are presented as a flowchart in Figure 1.

As shown in Figure 1, in the first step, a set of localized region-based features are extracted in each of the three visual image bands based on the nature of the required local features. Then, a set of primary matching features is determined, and unwanted and incorrect matches are eliminated using an innovative method introduced in this research. In the second step, a set of primary three-dimensional coordinate is computed for the initial matching points using the bundle adjustment. The geometric accuracy of the point coordinates is evaluated. Then, using the proposed MIP algorithm with a combination of geometric and radiometric properties of the points, the image coordinates are improved in a repetitive process. In the third stage, improved image points coordinates obtained from the MIP algorithm are entered into the displacement measurement stage using the CPDA method. The details of the processes for the proposed algorithm are described below.

2.1 Feature extraction algorithm

Based on the nature and type of application, local extraction algorithms can be divided into three categories. The first group extracts the features in such a way that according to the intended application, a specific interpretation can be considered for them. For example, extracting edges in aerial imagery can be related to road feature extraction, or extraction of image blobs can be used to identify non-similar areas with other areas of the image. Such algorithms can be used to extract specific features from the image. The second category is the applications that look at local features as a set of unique highly informative imagery points. In such applications, it is not of great importance what the extracted features demonstrate but the feature precise position and its stability in overlapping images with rotation, scale, or affine changes are important. Applications in this category include matching, moving body tracking, camera calibration, 3D modeling, image registration and orthophoto production. Finally, in the third category, the set of local features can be used as image component representatives. Image features and components can be identified using these representatives without the need for image segmentation. The application areas for this category include image classification, texture analysis, image retrieval,

Figure 1 Different steps of the proposed strategy and components of the proposed MIP algorithm

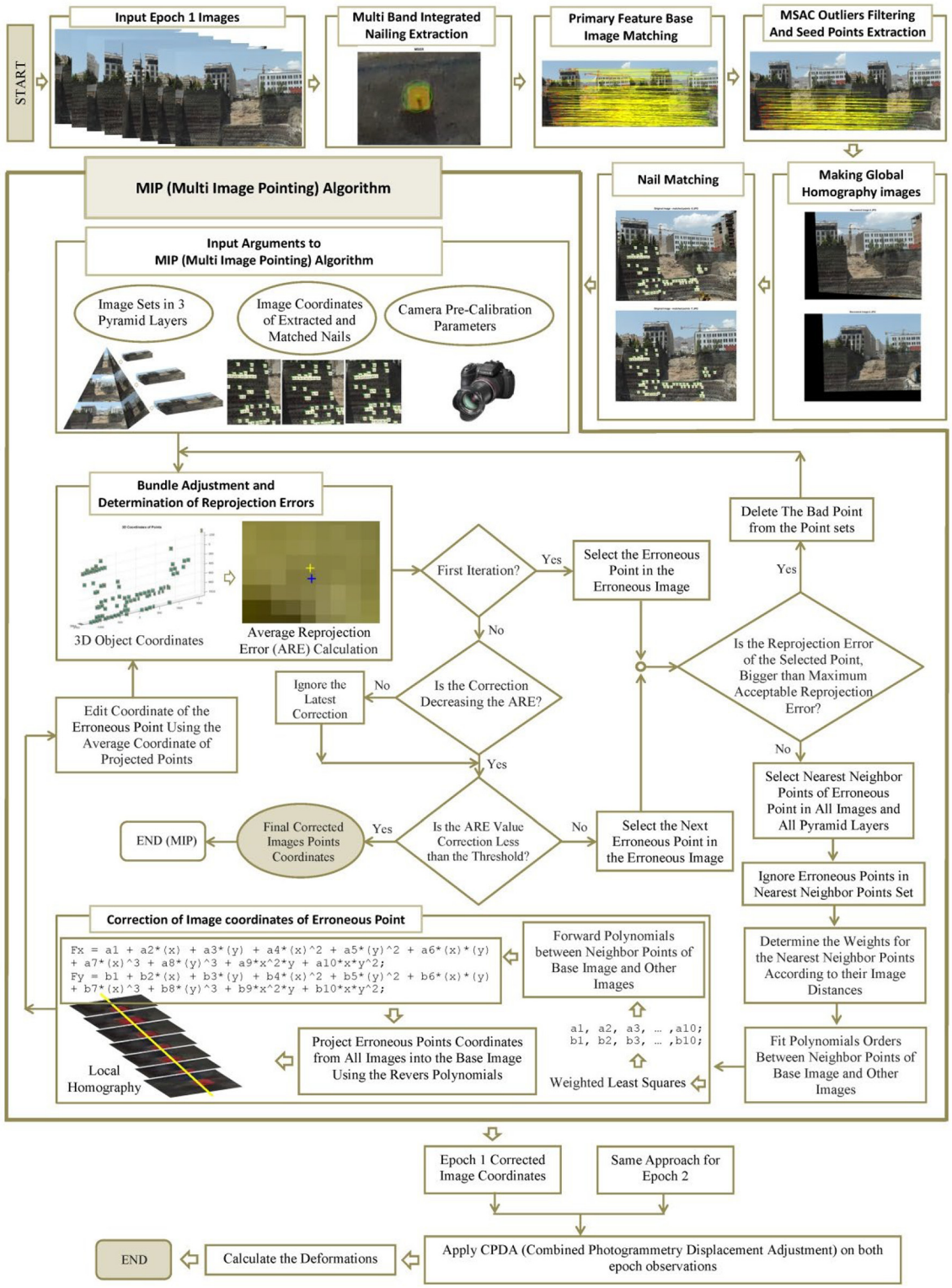

and video mining. In displacement measurements using photogrammetric methods, the second category is considered for the extraction of local features.

Common local features include points, blobs and visual areas. The most important point extraction algorithms are Harris (Harris and Stephens (1988)), SUSAN (Smith and Brady, 1997), Harris–Laplace and Harris-Affine (Lindeberg, 1993, 1998; Mikolajczyk and Schmid, 2004) and edge-based regions (Tuytelaars and Van Gool, 1999, 2004). The most popular blob extraction algorithms are Hessian, Hessian-Laplace, Hessian-Affine (Tuytelaars and Mikolajczyk, 2008) and salient regions (Kadir and Brady, 2001). Also, the most common image area extraction algorithms include intensity-based regions (Tuytelaars and Van Gool, 2000, 2004), maximally stable extremal regions (MSERs) and segmentation-based methods (Matas *et al.*, 2004). Regarding the implementation of these algorithms to investigate their performance and to extract local features from the excavation walls (Figure 2), as well as the inspiration from the results of studies by Tuytelaars and Mikolajczyk (2008), their performance can be ranked according to Figure 3.

According to Figure 3, the MSER algorithm is ranked higher in terms of the position accuracy for local-feature-extracted location because of the extraction of high-stability regions. Moreover, because of the nature of the soil nail excavation walls, in this study, the MSER algorithm was used as the basic algorithm for extracting local features required for the displacement measurement of excavation walls. The accuracy of the extracted feature utilizing this algorithm is improved using the MIP algorithm. After the MIP algorithm is applied to the base extractor results, local features will be ready to be used in the measuring displacement process.

2.2 Feature matching

Various algorithms have been defined for local feature matching on images (Bethmann and Luhmann, 2014; Bulatov *et al.*, 2011; Zhao *et al.*, 2018). The process of matching in the proposed algorithm is practically an innovative method to determine the corresponding nails in convergent images taken

Figure 3 Ranking and comparison among accuracy of local feature extraction algorithms

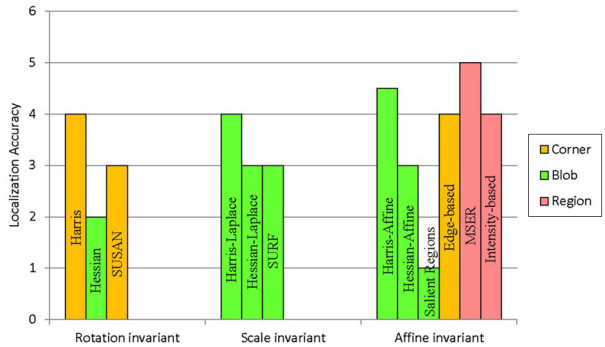

from the excavation walls. In the proposed algorithm, distinctive image features are extracted from the features in MSER areas for all images. These unique properties are based on the weighted image gradients around the center of gravity of the MSER areas (Lowe, 2004). Then, with a strict threshold limit, based on the strongest similar properties, the initial matches between the reference image and other images are determined. In the reference image, the angle of incidence for its optical axis bearing is closer to 90° compared to that of the other images. Initial matches are found using the matching threshold (representing a percent of the distance from a perfect match) and ratio threshold (denoting the matching percentage of the descriptor). These thresholds take different values for different image sets and should be determined empirically.

Based on the initial matching, the coefficients of a projective geometric transformation between the reference image and other images are determined. Initial matching points that do not conform to the threshold in the projective equations are eliminated. This mismatch elimination process is inspired by the M-estimator sample consensus algorithm (Hartley and Zisserman, 2003; Torr and Zisserman, 2000). Then, using the projective homography process, all the matched images and points are projected to the reference image. For the

Figure 2 Implementation of some local feature extractor on soil nail excavated walls and their qualitative performance comparison

Local feature	Point extraction			Blob extraction	Region extraction	
Extractor	Harris Detector	SUSAN Detector	Harris-Laplace	SURF	Segmentation-based Methods	Maximally Stable Extremal Regions (MSER)
Feature Extraction Result	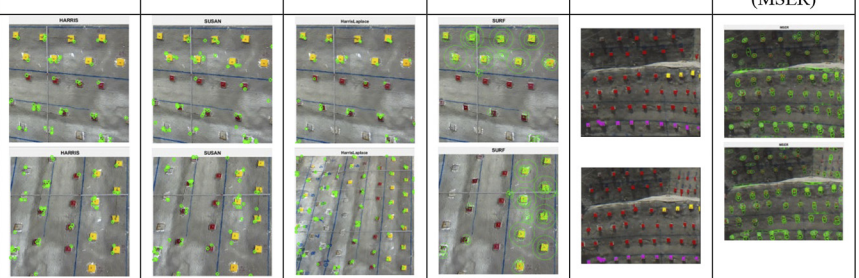					
Invariance	Rotation invariant	Rotation invariant	Rotation and Scale invariant	Rotation invariant	Affine invariant	Affine invariant

transformed matched points on the original image, the closest extracted point is determined by a strict threshold. Duplicate matches are eliminated based on the closest positions. Those features in the original image that have matching in all other images remain and their image and pixel coordinates, as well as the corresponding point numbers in all the images, are determined. This technique helps to conduct proper matching simultaneously for all images.

In both stages of extraction and matching, the algorithm's implementation stages are applied on three sets of images. As shown in Figure 4, the original image is located on the zero layer. The first-layer image with a resolution equal to half of the original image resolution and the image of the +1 layer with a resolution equal to twice the original image resolution are generated. In the image production of layers −1 and +1, the nearest-neighbor interpolation method is used to have the least change in the nature of the images. The MSER area extraction is performed on all three image layers. The use of an image pyramid in the local feature extraction reduces the effect of noise in the formation of the MSER area. In addition, the use of all three image pyramids in positioning the center of gravity of the MSER areas improves point extraction uncertainties and the accuracy of their geometric position. In other words, generating different boundaries for target local features, the pyramid layers enhance the chance of achieving the proper feature by the MSER algorithm. This is also partly the case in the application of all of the three bands of RGB.

The homography based matching process is performed on the original image set (layer 0), and in both layers −1 and +1 from the pyramid, similar points in the extracted positions, if any, are determined. In fact, the final matchings are obtained from the common results of extraction and matching processes in all three sets of image layers. Therefore, if there is no extraction or there exists a positional difference in two other layers in an MSER area, then the local feature is eliminated from the matching candidate list.

2.3 Multi-image pointing algorithm

The corresponding point set to the initial positions enters the main position improvement step with the proposed MIP algorithm. The steps in this algorithm, according to Figure 1, can be expressed as follows:

- The raw images along with generated ones in the pyramid +1 and −1 enter the algorithm as input data.
- Image and pixel coordinates of the points related to the extracted nail points with their corresponding numbers enter the algorithm.
- Camera calibration parameters enter the algorithm as pre-calibration input data.
- Initial modeling is performed for the points using primary coordinates, and the most erroneous point in the most erroneous image is determined based on the amount of reprojection error. The point where reprojection error is maximal is recognized as the most erroneous point, with the image containing this point considered as the most erroneous image. Then, sorting the corresponding image coordinates based on the highest reprojection error is performed [the reprojection error is the distance between the point coordinate detected in the image and the 3D point coordinate being reprojected to the image (Figure 5)].
- The closest extracted points to the erroneous point in the erroneous image (because of the fact that the points are corresponding to each other, these points are the same in all images) are determined based on the user-entered threshold (maximum pixel spacing). This step leads to the local point selection around the erroneous point and local implementation of the MIP algorithm in the image;
- From neighboring points, those falling in one-fourth of the highest reprojection error are eliminated.

Figure 5 Reprojection error; the distance between point detected in the image and 3D point reprojected into the image

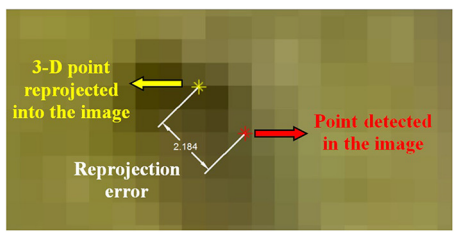

Figure 4 Image set generation in layers −1 and +1 using the original images

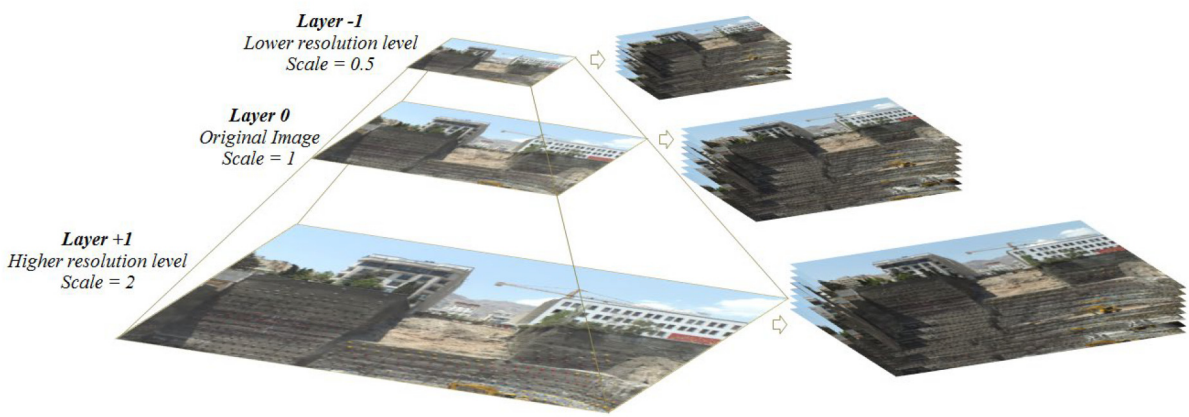

- The remaining neighboring points are weighted by the amount of proximity to the erroneous point. The nearest points will gain more weights and will have a greater impact on correcting the erroneous point coordinates.
- For each pyramidal layer, a polynomial is created (by weighted least squares method) from the points adjacent to the erroneous one in the erroneous image and the same points in other images [equation (1)]. The order of the polynomial is determined by the user based on the number of neighboring points. If there are more extracted matched points in the neighbor of erroneous point (according to the threshold), then the user can determine more polynomial orders. Erroneous points are not considered in determining the coefficients of this polynomial.

$$\begin{aligned} f_X &= a_1 + a_2x + a_3y + a_4x^2 + a_5y^2 + a_6xy + a_7x^3 + a_8y^3 \\ &\quad + a_9x^2y + a_{10}xy^2 \\ f_y &= b_1 + b_2x + b_3y + b_4x^2 + b_5y^2 + b_6xy + b_7x^3 + b_8y^3 \\ &\quad + b_9x^2y + b_{10}xy^2 \end{aligned} \tag{1}$$

The above equation is rewritten in each step between each image and the erroneous one. x and y are replaced by the coordinates of the points adjacent to the erroneous one on each image, f_x and f_y are set to the coordinates of the same points on the erroneous image. Then, coefficients $a_1, a_2, \ldots$ and $b_1, b_2, \ldots$ are determined using the weighted least squares adjustment method. In fact, a series of polynomial coefficients are calculated between each image and the erroneous one.

For obtaining the coefficients in the polynomial, observation equations are formed according to equation (2):

$$\begin{matrix} \mathrm{L=AX} \\ L \qquad\qquad A \qquad\qquad X \end{matrix}$$

$$\overbrace{\begin{bmatrix} X_1 \\ X_2 \\ . \\ . \\ X_i \end{bmatrix}}^{L} = \overbrace{\begin{bmatrix} 1 & x_1 & y_1 & {x_1}^2 & . & . & x_1{y_1}^2 \\ 1 & x_2 & y_2 & {x_2}^2 & . & . & x_2{y_2}^2 \\ . & . & . & . & . & . & . \\ . & . & . & . & . & . & . \\ 1 & x_i & y_i & {x_i}^2 & . & . & x_i{y_i}^2 \end{bmatrix}}^{A} \overbrace{\begin{bmatrix} a_1 \\ a_2 \\ . \\ . \\ a_{10} \end{bmatrix}}^{X} \tag{2}$$

where i is the number of points adjacent to the erroneous one, L is the X or Y coordinate matrix of the points adjacent to the erroneous one on the erroneous image, and A is the x and y coordinate matrix of the points adjacent to the erroneous one on each image based on the terms in the polynomial. X is the coefficient matrix of the polynomial ($a_1, a_2, \ldots$ or $b_1, b_2, \ldots$), which is unknown, and is determined with the weighted least squares adjustment method according to equation (3):

$$\hat{X} = (A^T PA)^{-1} A^T PL \tag{3}$$

where P is the observation weight matrix, in which a value between 0 and 1 is inserted for each point based on the image distance from that point to the erroneous one. Closer points are more effective in improving the coordinates of the erroneous point. $\hat{X}$ is the estimated coefficient of the polynomial. L and A are the same as in equation (2).

- After calculation of the coefficients in the polynomial between the points adjacent to the erroneous one between each image and the same points on the erroneous image, the erroneous point on each image is projected onto the erroneous image based on the polynomial formed for it. That is, x and y are replaced in equation (1) this time by the coordinates of the erroneous point on each image, and the coordinates of its projection on the erroneous image, namely, f_x and f_y, are obtained using the coefficients calculated in the previous step.
- This process is performed on all three image pyramids (the image in layer −1 of pyramidal image minimizes the effect of regional noise in the image that changes the image coordinates of the nail center).
- Using the weighted average of the locations of the erroneous points projected from all the images in all the pyramid layers onto the erroneous image, the coordinates are updated on the erroneous image [equation (4)].

$$\begin{aligned} X_{Corr} &= \frac{\frac{\sum_{i=1}^{n-1} x_{i(L_{-1})}}{n-1} + 2\frac{\sum_{i=1}^{n-1} x_{i(L_0)}}{n-1} + \frac{\sum_{i=1}^{n-1} x_{i(L_1)}}{n-1}}{4} \\ Y_{Corr} &= \frac{\frac{\sum_{i=1}^{n-1} y_{i(L_{-1})}}{n-1} + 2\frac{\sum_{i=1}^{n-1} y_{i(L_0)}}{n-1} + \frac{\sum_{i=1}^{n-1} y_{i(L_1)}}{n-1}}{4} \end{aligned} \tag{4}$$

In the above equation, X_{Corr} and Y_{Corr} are the corrected coordinates of the erroneous point, n is the number of images, $x_{i(L_{-1})}$ is the x coordinate of the erroneous point projected from the ith image onto the erroneous image in pyramid layer −1, L_{-1} is the pyramid layer −1, L_0 is pyramid layer 0 and L_1 is pyramid layer 1. The effect of the corrected coordinates from the main pyramid layer (0) has been increased in the calculation of the final coordinates of the erroneous point through the inclusion of coefficient 2.

- The algorithm continues to run until there is not any improvement of the average reprojection error (ARE) in an effective MIP cycle in a specific threshold.

After applying MIP algorithm on image observations, it can be ensured that the effects of the various image conditions (discussed in Section 1) on erroneous image observations have been largely overcome, and these observations can be utilized for the displacement measurement process.

2.4 Deformation detection

After improving the positions, the image coordinates that have been improved individually using the image equations for each epoch are included in the displacement measurement step.

In the soil nail walls, according to Federal Highway Administration laws, the maximum allowable horizontal and vertical displacement above a nailing wall depends on the wall height and is estimated by equation (5) (Lazarte *et al.*, 2003):

$$\delta h = (\delta_h/H)i \times H \quad (5)$$

where δ_h is the maximum horizontal displacement at the top of the wall (Figure 6), H is the wall height and $(\delta_h/H)i$ is the coefficient determined based on the soil type according to Table 2 (Lazarte *et al.*, 2003). In addition, the horizontal distance behind the nailing wall, which is affected by the displacement of the wall, is determined by a factor of the wall height and the vertical inclination angle using equation (6) (Lazarte *et al.*, 2003):

$$D_{DEF} = C \times H \times (1 - \tan\alpha) \quad (6)$$

where D_{DEF} is the horizontal distance behind the wall, which is affected by the wall displacement (Figure 6), H and α are the wall height and the vertical inclination angle, respectively, and C is the coefficient that according to the soil type is determined from Table 2 (Lazarte *et al.*, 2003). For example, in this research, for a perfectly vertical excavation with a height of 25 m and sandy soil, the maximum allowable displacement at the top of the wall is 5 cm and the distance behind the wall affected by the displacement will be 20 m. Therefore, determining displacements with an accuracy of 1–2 cm will be very valuable.

In conventional measuring displacement techniques such as micro-geodesy and the use of the global positioning system, the observations are carefully selected and adjusted in two distinct epochs to measure changes in the position of the points as a representative of the feature. Then, the point sets are subjected to a 3D transformation into a single coordinate system using a series of observed points that are fixed and not displaced in both epochs. Finally, the displacement is determined by comparing the coordinates of the corresponding displaced points. However, based on the conducted evaluations (Esmaeili *et al.*, 2013), such a measuring displacement structure in close-range photogrammetry does not produce the proper accuracy in the results of displacement measurements. In other words, when two epochs having different grid structures and different errors are adjusted, the accuracy of determining the reference point coordinates (Figure 3), which are fixed in both epochs, will be different. When these points are used as reference points to match the coordinates of the two epochs, the accuracy of the displacement will be affected by the accuracy differences in the coordinate determination of these points and their location in the observed points and consequently unrealistic results will be obtained. Reference fixed points are considered on fixed features outside the area affected by displacement according to equation (6).

Therefore, according to the research carried out by Esmaeili *et al.* (2013), simultaneous combined adjustment of both epochs is proposed with the assumption of joint observations for the reference points in both epochs and independent observations in each epoch for displaced points. In this method, the network generated by the first epoch with the corresponding interior orientation, along with the network generated by the second epoch with the interior orientation of the second network, is simultaneously adjusted. For fixed points, the coordinates are commonly determined between the two epochs, and for the displaced points, the corresponding epoch images are used (Esmaeili *et al.*, 2013). Therefore, as the output of this method, a set of coordinates for fixed points and two sets of coordinates for displaced points are all determined in a common coordinate system. These two coordinate sets of displaced points are related to the first and second epochs. By comparing the coordinates of these displaced points, the amount of displacement in two epochs is obtained. This method is known as CPDA (Esmaeili *et al.*, 2013).

In this case, scale bars are used to fit the measurements in actual scale. An important point about the displacement measurement of the soil nail excavated walls is the continuous change in the wall surface because of the wall collapse or shotcrete of the subsequent excavation layers. Therefore, except the metal plate of the nails, which are first stained and continuously washed after each shotcrete, other wall sections are not in constant condition. This makes it impossible to use surface modeling and comparisons to determine the wall's behavior by using the photogrammetric method for displacement measurement because most changes will be due to the changes in the shotcrete thickness in different stages of cementation rather than wall displacements.

All stages of extraction, matching, accuracy improvement and displacement measurements were specifically designed for the excavation walls. Therefore, to facilitate the entire work, all these steps were presented in the form of a user interface called

Figure 6 Deformation of soil nail walls

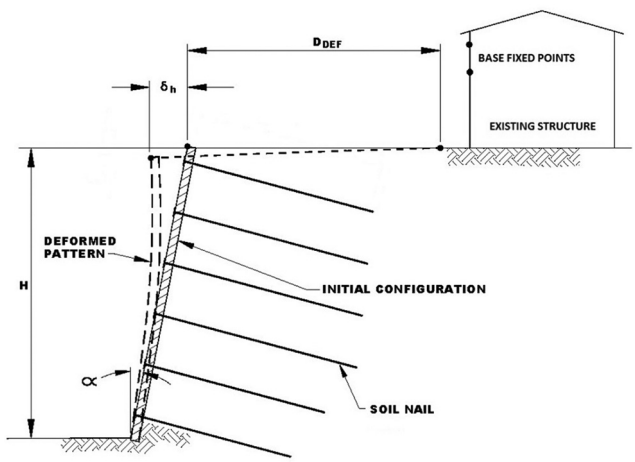

Source: Lazarte *et al.* (2003)

Table 2 Values of $(\delta_h/H)i$ and C as functions of soil conditions "i"

Variable	Weathered rock and stiff soil	Sandy soil	Fine-grained soil
$(\delta_h/H)_i$	1/1000	1/500	1/333
C	1.25	0.8	0.7

Source: Lazarte *et al.* (2003)

Farid excavation deformation detection using MATLAB software.

3. Experimental results

The performance of the proposed algorithm was evaluated in the form of a real excavation project. To evaluate the accuracy of the algorithm results, the displacements measurement was compared with the displacements measured by micro-geodesy and target-based photogrammetric methods. In the following, the results of this project are described.

3.1 Soiled nail excavation project

The project under study was the stabilization of the 35-m-deep excavation for Behesht-e-Zaferranie commercial complex project. This project is located on the 13th Velenjak Street, located in the 1st municipality district of Tehran, Iran. The land area dimension in this project is 33.5 × 58.35 m. The excavation depth at the northern wall is 35 m from the current status before excavation and from the street level is 25 m. In general, the excavation, where soil nailing is used to reinforce the walls, is performed step-by-step. At each excavation stage, the nailing system that has been designed by civil engineers according to the project conditions is implemented on the walls. Figure 7 shows two stages of excavation in the project under study.

To investigate and evaluate the results of the proposed algorithm, the displacement measurement of the excavated wall in two epochs was performed applying the photogrammetric method in two different ways: using photogrammetric targets and using extracted and improved local features utilizing the proposed MIP algorithm. In addition, to verify the accuracy of the results, micro-geodesy observations were performed simultaneously for both epochs. In this method, the distance and angle observations were made from three fixed stations positioned on the street opposite to the wall with an allowable distance away from wall displacements effect, using total station instrument. It should be noted that in excavation walls reinforced by soil nailing method, the displacement measurement cannot be performed using wall surface modeling and observed surface comparison in different epochs. The main reason is that after each excavation step, wall shotcrete is performed, and because of this added shotcrete layers in each step, the wall thickness will vary in different parts. These changes are different from changes because of wall displacement and wall surface cannot be used for displacement measurement.

Figure 7 Progress of the project under study in two epochs

Close-range photogrammetry imaging was performed across a convergent networkusing 20–25 images per epoch. For this purpose, a Fujifilm Digital Camera FINEPIX HS20EXR was used and the images were taken at a focal length of 5 mm (Figure 8). Considering limitations in the project space, the average distance between imaging stations and feature was 58 m and the average scale of the images was 1:12,000, making up a ground sample distance of about 16 mm.

According to the empirical equation of error propagation, the accuracy of estimation of ground points in each epoch is predicted to be within 4 mm by equation (7).

$$\overline{\sigma}_c = \frac{q}{k^{1/2}} S\sigma \rightarrow \overline{\sigma}_c = \frac{0.7}{\sqrt{2}} \times 12000 \times 0.5 \times 1.38 \times 10^{-6} = 0.004 \quad \text{m} \tag{7}$$

In this equation, $\overline{\sigma}_c$ is the average standard deviation of associated error with XYZ coordinates of object points and q is the design factor or geometrical robustness coefficient of the network. In this project, the value of q was assumed as 0.7. The parameter k denotes the average number of images taken per imaging station, which was 2 in this project. S refers to the average scale of images, which is 1:12,000 in this project. σ represents the average xy coordinate error of image points, which was herein considered as 0.5 pixel. Each pixel on the sensor has a dimension of 0.00138 mm.

3.2 Extracting image points

The displacement measurement of the excavated walls was performed by using photogrammetric targets and using the local region-based features, which was extracted by the MSER algorithm and improved with the proposed MIP algorithm. Using the MIP method, the initial extraction of image points in the form of nails extraction was performed using the MSER algorithm. The MSER areas were extracted with appropriate

Figure 8 Technical characteristics of the used camera

Fujifilm Digital Camera FINEPIX HS20EXR

Type
16 Megapixel,1/2-inch EXR **CMOS** with primary color filter - sensor size : 6.40 × 4.80 mm
Focal Length
f = 4.2 - 126mm, equivalent to 24-720mm on a 35mm camera
Number of Recording Pixels
4608 × 3456 (4:3)

thresholds. Then, an ellipse was fitted to these regions of pixels and the central point of this ellipse was extracted as an image point. Because of the radiometric differences of the nail plate, the extraction of the MSER areas occurred in all three RGB bands, and the common extracted positions with a threshold were considered as the final points in each image. Figure 9 shows an example of the extracted regions for all three image bands. Also, to reduce the effect of image noise and increase the stability of the final point positions derived from the MSER areas, as described in section 2.2, the area extraction was performed in all three layers from the image pyramid.

In the target-based approach, two photogrammetric sets of reflector targets were used. The first set was installed on the wall for tracking with a diameter of 14 cm and an average of 30 m from the camera positions. The second set was installed on the building wall behind the excavation wall (32 m away from the wall), which was located far from the distance affected by displacements (minimum distance: 20 m) according to equation (6) [Figure 10(d)]. The target diameter was 16 cm and placed at an average distance of 80 m from the camera positions. The extraction of the image coordinates of these target centers was performed using the regional segmentation algorithm based on region growth. Figure 10(a) illustrates an example of these targets and their central coordinate extraction. To prevent targets from being covered with shotcretes, they were covered with nylon in the early stages [Figure 10(c)]. Also, micro-geodesy targets were installed along with some

Figure 9 Extraction of the MSER areas and central points

Notes: (a) Red band; (b) blue band; (c) green band

Figure 10 (a) S sample of photogrammetry target used and its center point extraction. (b) Micro-geodesy targets installed along with photogrammetric target. (c) Meshing, drainage and shotcrete of a part of the wall and temporary covering of photogrammetric targets with nylon to prevent the cement spray on them. (d) Base targets

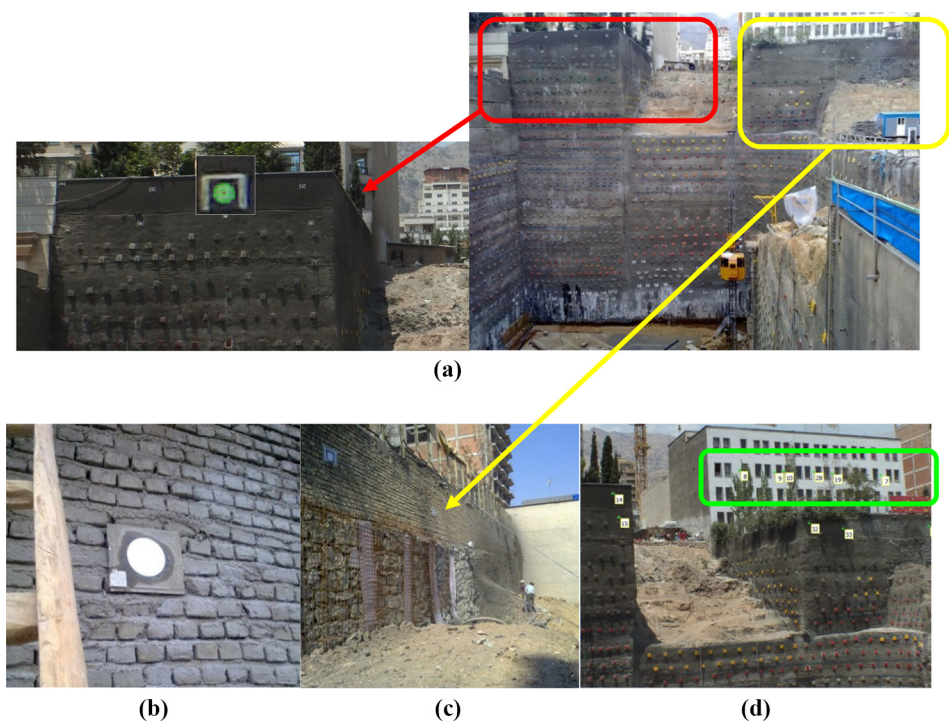

photogrammetric targets to verify the amount of displacement [Figure 10(b)].

3.3 Matching points

After the points were extracted, the nail matching was carried out according to the strategy described in section 2.2. Figure 11(a) depicts dense matching with noise elimination between two images of the acquired converging image collection. Figure 11(b) and 11(c) illustrates the homographic images generated from property-based matching results. Figure 12 depicts the final results of nail matching between two samples from a convergent image set of the feature in two epochs.

3.4 Multi-image Pointing algorithm implementation

To improve the accuracy of image coordinates and prepare the extracted corresponding points for displacement measurement, MIP algorithm was introduced and implemented. According to the algorithm described in Section 2–3, after determining the initial point coordinates, the observations were sorted according to the

Figure 11 Extraction of MSER areas and central points

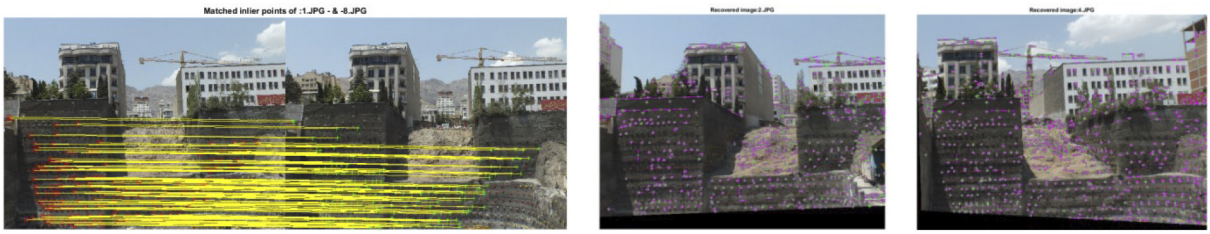

(a) (b) (c)

Notes: (a) Corrected dense matching; (b, c) two samples of created homograph images

Figure 12 (a) Sample of nail extraction and matching in the first epoch's images; (b) sampling and nail sampling in the second epoch's image

(a)

(b)

reprojection error value were entered individually into the MIP algorithm in each cycle. The process continued to the point where the MIP's effective cycle could not improve the results of the 3 D point coordinates based on a predefined threshold. Also, in some cycles, when the process of changing the image coordinates of the erroneous points through the MIP algorithm did not improve, the effect of applied changes was removed and that algorithm cycle was eliminated as an ineffective repetition of the process.

Since bundle adjustment was performed using the least-squares method, therefore, each time the process was executed, the mean error would be different from the previous one. But what in all program executions could be noticed is the reduction of the mean value for the reprojection error in effective MIP cycles. Figure 13 shows the geometric accuracy of the feature-based photogrammetric network in both epochs in the Velenjak project observations in both cases including scenarios of without using the MIP algorithm and also using the MIP algorithm.

As shown in Figure 13, the geometric accuracy of the network increases with the use of the MIP algorithm by correcting the image observation positions at each step and replacing them with the previous observations. This increase in accuracy in the ARE parameters can be detected in the first epoch observations to 0.2 pixels and the second epoch observations to 0.6 pixels. This increase in precision is directly related to the precision of determining the location of 3D point coordinates and consequently will result in an increase in the displacement measurement accuracy between the two effective epochs. Figure 14 illustrates the final 3D coordinates of the first epoch points in the last effective repetition of the MIP algorithm as well as the exterior orientation parameters of the camera.

3.5 Displacement measurement using the combined photogrammetry displacement adjustment method and evaluating the results

After improving the image coordinates accuracies of the extracted points using the MIP algorithm, observations were ready to enter the measuring displacement phase. As noted in Section 4.2, for the displacement measurement between the two epochs, both sets of observation epochs were adjusted simultaneously using the CPDA method. This simultaneous measuring displacement was performed using the MIP-based

Figure 14 Refined 3D points and camera positions using seven images

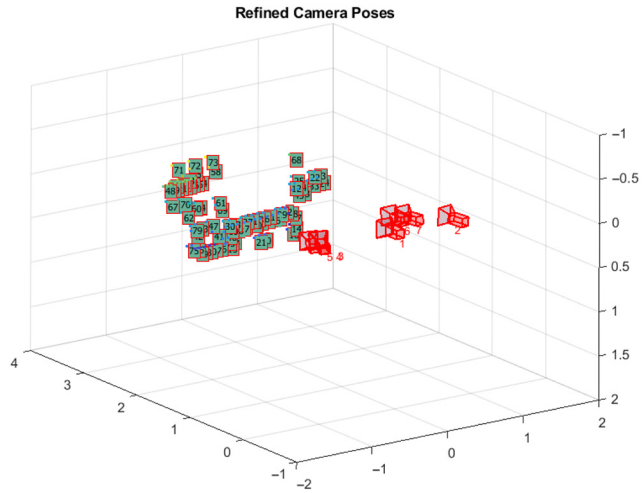

photogrammetry and target-based photogrammetry as well as micro-geodesy methods. The interior orientation parameters of the imaging camera (Fujifilm Digital Camera FINEPIXHS20EXR9) were determined by the pre-calibration method in a test-field appropriate to the feature scale at the project location. The estimation precision of point geo-coordinates and their mean value in the photogrammetric network, which was adjusted using the CPDA method, in X, Y and Z directions are presented in Table 3.

According to Table 3 for the target-based photogrammetry method, the Precision of the network is about 3 mm and 8 mm for the MIP-based photogrammetry method, respectively. According to equation (7), the accuracy of the estimation of ground points in each epoch was predicted to be 4 mm. So, according to Table 3 and equation (7), the accuracy of estimation of ground points in the target-based photogrammetry network adjusted by the CPDA method (3 mm), is approximately the same as the predicted one. But in the MIP-based photogrammetry network, because of the non-use of targets, the accuracy obtained is slightly different from

Figure 13 Diagram showing the variation in ARE in two states: using MIP and not using the MIP algorithm

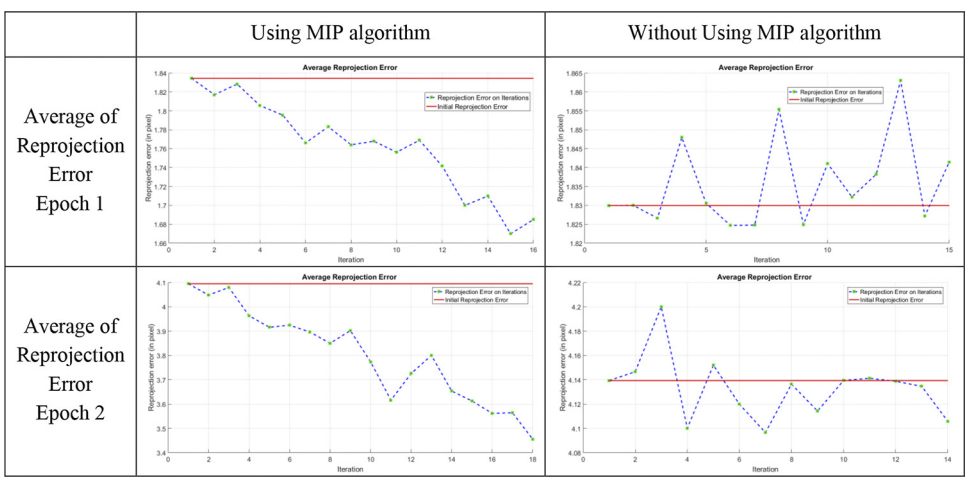

Table 3 Network proration precision between two epochs for displacement monitoring using the CPDA method (units in m)

Mrthod/ Precision	Target-based photogrammetry	MIP-based photogrammetry	Micro-geodesy
Precision (*X*)	0.003	0.006	0.003
Precision (*Y*)	0.004	0.007	0.003
Precision (*Z*)	0.002	0.011	0.005
Overall	0.003	0.008	0.004

the predicted accuracy but is acceptable with respect to the amount of displacement.The precision of the micro-geodesy network was about 4 mm considering the network created in the opposite street and the coordinate differences in a fixed point set in several epochs. To determine and evaluate the accuracy of the results, the average point displacement on the wall between two epochs was determined by applying different methods. These results are shown in Table 4.

In Table 4, the absolute average differences (AAD) between the measured displacement of the common points using two methods of micro-geodesy and photogrammetry (target-based photogrammetry or MIP-based photogrammetry) is presented using equation (8).

$$\mathrm{AAD} = \frac{\sum_{i=1}^{n} |d(x,y,z)_i - \acute{d}(x,y,z)_i|}{n} \tag{8}$$

where $d(x, y, z)_i$ is the displacement vector length defined for the ith point between two epochs in the micro-geodesy method. $d'(x,y,z)_i$ is the displacement vector length defined for the ith point between two epochs by the photogrammetric method; n is the number of points on the wall, where the displacement measurement was carried out. According to Table 4, if the displacement value determined by the micro-geodesy method between the two epochs is set as the basis, the displacement determined using photogrammetric targets differs by a 3 mm compared with that of the micro-geodesy method. The displacement determined by the simple point extraction without using the MIP algorithm is 3 cm with respect to the micro-geodesy method. However, in the case of using the proposed MIP algorithm for correcting and improving the image coordinates of the extracted points, the displacement differences compared with that of the micro-geodesy method were 9 mm. The mean difference between measured point displacements in target-based photogrammetric method and micro-geodesy was about 8 mm. The average difference between measured point displacements using the proposed MIP algorithm and micro-geodesy was about 13 mm. The results indicate that although the use of photogrammetric targets has yielded more accurate results, if these targets are not used, the proposed MIP algorithm can greatly cope with the required accuracy in such projects using local features on the structure. Given the excavation wall height in the second epoch, H = 20m, and the dominant soil type as sandy ($(\delta_h/H)i$ = 1/500 according to Table 2), based on equation (5) and Table 2, the maximum expected allowable displacement is equal to:

$$\delta h = (\delta_h/H)i \times H \quad \rightarrow \delta_h = \frac{1}{500} \times 20 = 0.04\,\mathrm{m} = 4\,\mathrm{cm} \tag{9}$$

According to equation (9), if displacements between two epochs are greater than 4 cm, the project becomes out of the normal condition and some preventive measures must be considered such as truss construction, shortening nail spacing, increasing nail length or using other auxiliary methods such as the reciprocal support or the use of anchoring. These preventive actions need to be carried out during the project progress to prevent the wall collapse. This amount of critical displacement, 4 cm, can be easily determined using the proposed measuring displacement method, MIP algorithm. Therefore, the proposed method was able to provide the required accuracy for displacement measurement in the project.

If there is a possibility of accessing to the cracks created by the wall movement, one of the traditional methods of monitoring the cracks is to plaster on the part of the crack created behind the wall and put the date on it. If the cracking diameter increases in the wall, the plaster will also slot on it. By measuring the created gap, the amount of displacement created in the structure will be determined. Figure 15 shows the crack plastering in this project.

According to the results of this method between the two measurement epochs, the average wall displacement of approximately 3 cm was confirmed with the plastering method.

Table 4 Results of determining the average displacement of the wall between two epochs by micro-geodesy methods, target-based photogrammetry, photogrammetry without using the MIP method and the proposed method of MIP photogrammetry (units in m)

Mean of displacement on the wall (micro-geodesy)	Mean of displacement on the wall (target-based photogrammetry)	Mean of displacement on the wall (simple points extraction – no usage of the MIP algorithm)	Mean of displacement on the wall (MIP-based photogrammetry)	AAD between micro-geodesy and (target-based photogrammetry)	AAD between micro-geodesy and (MIP-based photogrammetry)
0.031	0.034	0.061	0.040	0.0077	0.0128

Figure 15 Plastering the cracks and comparing the crack dimensions on plaster at different timeframes to acquire a field estimation of the displacement

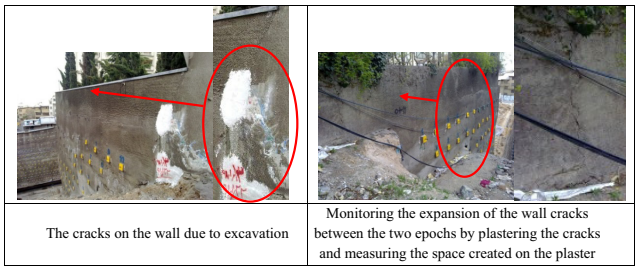

The cracks on the wall due to excavation	Monitoring the expansion of the wall cracks between the two epochs by plastering the cracks and measuring the space created on the plaster

4. Conclusions

The displacement measurement of large scale structures, such as excavated walls is of great importance because of providing structural behavior monitoring and consequently the prevention of accidents. Applying commonly used methods, such as micro-geodesy and instrumentation, have limitations such as high cost, difficulty in implementation and time-consuming observations. Photogrammetric methods that use the local features on the structure as the reference point displacement measurements, requires high accuracy in the point extraction and matching. Some Limitations of photogrammetry include: parallax, poor feature texture and radiometric differences between images cause that the position of the corresponding local features extracted in the images does not have the appropriate geometric accuracy to be used as the basis for the displacement measurement. Therefore, in this paper, the new MIP algorithm based on the geometric characteristics of the model generated from the initial matching was introduced, which, in a self-adaptive way, corrected the extracted image coordinates. The unique characteristic of this proposed algorithm was that the position correction was accomplished with the help of continuous interaction between the 3D model coordinates and the image coordinates and had the least dependency on the geometric and radiometric nature of the images. After the initial feature extraction and implementation of the MIP algorithm, the image coordinates were ready for use in the displacement measurement process. The CPDA algorithm was used for displacement measurement between two epochs. Micro-geodesy, target-based photogrammetry and the proposed MIP methods were used in a displacement measurement project for an excavation wall in the Velenjak area in Tehran, Iran to evaluate the proposed algorithm performance. According to the results, the measurement accuracy of the point geo-coordinates of 8 mm and the displacement accuracy of 13 mm could be achieved using the MIP algorithm. In addition to the micro-geodesy method, the accuracy of the results was matched by the cracks created behind the project's wall. Given the maximum allowable displacement limit of 4 cm in this project, the use of the MIP algorithm produced the required accuracy to determine the critical displacement in the project. Some advantages of the proposed MIP photogrammetry algorithm, including the ease of obtaining observations and using local features on the structure in the images rather than installing the artificial targets, make it possible to effectively replace micro-geodesy and instrumentation methods. In addition, the proposed MIP method is superior to the target-based photogrammetric method as it does not need artificial target installation and protection. Moreover, in each photogrammetric application that needs to determine the exact point coordinates on the feature, the proposed algorithm can be very effective in providing the possibility to achieve the required accuracy according to the desired objectives.

Notes

1 Combined photogrammetry displacement adjustment.

2 Refined distance constraint.

3 Finite Element Method.

References

Alba, M., Barazzetti, L., Giussani, A., Roncoroni, F. and Scaioni, M. (2010), "Development and testing of a method for tunnel monitoring via vision metrology", *The International Archives of Photogrammetry, Remote Sensing and Spatial Information Sciences*, Vol. XXXVIII No. 5.

Barazzetti, L. and Scaioni, M. (2010), "Development and implementation of image-based algorithms for measurement of deformations in material testing", *Sensors*, Vol. 10 No. 8, pp. 7469-7495, doi: 10.3390/s100807469.

Bethmann, F. and Luhmann, T. (2014), "Object-based multi-image semi-global matching – concept and first results", International Archives of the Photogrammetry, Remote Sensing and Spatial Information Sciences - ISPRS Archives, doi: 10.5194/isprsarchives-XL-5-93-2014

Bulatov, D., Wernerus, P. and Heipke, C. (2011), "Multi-view dense matching supported by triangular meshes", *ISPRS Journal of Photogrammetry and Remote Sensing*, Vol. 66 No. 6, pp. 907-918, doi: 10.1016/j.isprsjprs.2011.06.006.

Cerminaro, D.J. (2014), *Implementation of Photogrammetry to Improve Proactive Assessment of Retaining Walls along Transportation Corridors*, MI Technological University MI.

Esmaeili, F., Varshosaz, M. and Ebadi, H. (2013), "Displacement measurement of the soil nail walls by using close range photogrammetry and introduction of CPDA method", *Measurement*, Vol. 46 No. 9, pp. 3449-3459, doi: 10.1016/j.measurement.2013.04.069.

Esmaeili, F., Ebadi, H., Saadatseresht, M. and Kalantary, F. (2019b), "Application of UAV photogrammetry in displacement measurement of the soil nail walls using local features and CPDA method", *ISPRS International Journal of Geo-Information*, doi: 10.3390/ijgi8010025.

Esmaeili, F., Ebadi, H., Mohammadzade, A. and Saadatseresht, M. (2019a), "Evaluation of close-range photogrammetric technique for deformation monitoring of large-scale structures: a review", *Journal of Geomatics Science and Technology*, Vol. 1.

Feng, T., Mi, H., Scaioni, M., Qiao, G., Lu, P., Wang, W. and Tong, X. (2016), "Measurement of surface changes in a scaled-down landslide model using high-speed stereo image

sequences", *Photogrammetric Engineering & Remote Sensing*, Vol. 82 No. 7, pp. 547-557, doi: 10.14358/PERS.82.7.547.

Fraser, C. (1999), "Automated vision metrology: a mature technology for industrial inspection and engineering surveys", *6th South East Asian Surveyors Congress*.

Fraser, C. (2001), "Automated vision metrology:a mature technology for industrial inspection and engineering surveys", *Australian Surveyor*, Vol. 46 No. 1, pp. 5-11, doi: 10.1080/00050355.2001.10558822.

Fraser, C.S. and Riedel, B. (2000), "Monitoring the thermal deformation of steel beams via vision metrology", *ISPRS Journal of Photogrammetry and Remote Sensing*, Vol. 55 No. 4, pp. 268-276, doi: 10.1016/S0924-2716(00)00024-1.

Fraser, C., Brizzi, D. and Hira, A. (2003), "Vision-based, multi-epoch deformation monitoring of the atrium of federation square", *11th FIG Symposium on Deformation Measurements*, *Santorini*.

Fraser, C.S., Woods, A. and Brizzi, D. (2005), "Hyper redundancy for accuracy enhancement in automated close range photogrammetry", *The Photogrammetric Record*, Vol. 20 No. 111, pp. 205-217, doi: 10.1111/j.1477-9730.2005.00327.x.

Harris, C. and Stephens, M. (1988), "A combined corner and edge detector", *Alvey Vision Conference*, pp. 147-151.

Hartley, R. and Zisserman, A. (2003), *Multiple View Geometry in Computer Vision*, second edi., Cambridge University Press, New York, NY.

Jiang, R. (2005), *Development of a Digital Photogrammetric System for Bridge Deflection Measurement*, NM State University Mexico.

Jiang, R. and Jauregui, D.V. (2010), "Development of a digital close-range photogrammetric bridge deflection measurement system", *Measurement*, Vol. 43 No. 10, pp. 1431-1438, doi: 10.1016/J.MEASUREMENT.2010.08.015.

Kadir, T. and Brady, M. (2001), "Saliency, scale and image description", *International Journal of Computer Vision*, Vol. 45 No. 2, pp. 83-105, doi: 10.1023/A:1012460413855.

Lazarte, C.A., Elias, V., Espinoza, R.D. and Sabatini, P.J. (2003), *Geotechnical Engineering Circular No. 7: Soil Nail Walls*, Federal Highway Administration, Washington, DC, MD.

Lee, T.K. and Al-Mahaidi, R. (2008), "An experimental investigation on shear behaviour of RC T-beams strengthened with CFRP using photogrammetry", *Composite Structures*, Vol. 82 No. 2, pp. 185-193, doi: 10.1016/J.COMPSTRUCT.2006.12.012.

Li, C. and King, B. (2002), "Close range photogrammetry for the structural monitoring of the star ferry colonnade", *Geology*, Vol. 4 No. 2, pp. 135-143.

Li, L., Zhang, X., Chen, G. and Lytton, R. (2015), "Measuring unsaturated soil deformations during triaxial testing using a photogrammetry-based method", *Canadian Geotechnical Journal*, Vol. 53 No. 3, pp. 472-489, doi: 10.1139/cgj-2015-0038.

Lindeberg, T. (1993), "Detecting salient blob-like image structures and their scales with a scale-space primal sketch: a method for focus-of-attention", *International Journal of Computer Vision*, Vol. 11 No. 3, pp. 283-318, doi: 10.1007/BF01469346.

Lindeberg, T. (1998), "Feature detection with automatic scale selection", *International Journal of Computer Vision*, Vol. 30 No. 2, pp. 79-116, doi: 10.1023/A:1008045108935.

Lowe, D.G. (2004), "Distinctive image features from scale-invariant keypoints", *International Journal of Computer Vision*, Vol. 60 No. 2, pp. 91-110, doi: 10.1023/B:VISI.0000029664.99615.94.

Luo, X., Tan, H., Lin, G. and Lian, Y. (2017), "Strain field measurements using digital photogrammetry for large inflatable structures", *Experimental Techniques*, Vol. 41 No. 5, pp. 453-462, doi: 10.1007/s40799-017-0190-5.

Matas, J., Chum, O., Urban, M. and Pajdla, T. (2004), "Robust wide-baseline stereo from maximally stable extremal regions", *Image and Vision Computing*, Vol. 22 No. 10, pp. 761-767, doi: 10.1016/J.IMAVIS.2004.02.006.

Mikolajczyk, K. and Schmid, C. (2004), "Scale & affine invariant interest point detectors", *International Journal of Computer Vision*, Vol. 60 No. 1, pp. 63-86, doi: 10.1023/B:VISI.0000027790.02288.f2.

Miller, P.E. (2009), Applications of 3D measurement from images, *The Photogrammetric Record*, Vol. 24, Whiltles Publishing, Scotland, doi: 10.1111/j.1477-9730.2009.00545_1.x

Oats, C.R., Escobar-Wolf, R. and Oommen, T. (2017), "A novel application of photogrammetry for retaining wall assessment", in *Infrastructures*, Vol. 2 No. 3, p. 10, doi: 10.3390/infrastructures2030010.

Ozbek, M., Rixen, D.J., Erne, O. and Sanow, G. (2010), "Feasibility of monitoring large wind turbines using photogrammetry", *Energy*, Vol. 35 No. 12, pp. 4802-4811, doi: 10.1016/J.ENERGY.2010.09.008.

Scaioni, M., Feng, T., Barazzetti, L., Previtali, M. and Roncella, R. (2015), "Image-based deformation measurement", *Applied Geomatics*, Vol. 7 No. 2, pp. 75-90, doi: 10.1007/s12518-014-0152-x.

Scaioni, M., Barazzetti, L., Giussani, A., Previtali, M., Roncoroni, F. and Alba, M.I. (2014), "Photogrammetric techniques for monitoring tunnel deformation", *Earth Science Informatics*, Vol. 7 No. 2, pp. 83-95, doi: 10.1007/s12145-014-0152-8.

Schmid, C. and Mohr, R. (1997), "Local grayvalue invariants for image retrieval", *IEEE Transactions on Pattern Analysis and Machine Intelligence*, Vol. 19 No. 5, pp. 530-535, doi: 10.1109/34.589215.

Smith, S.M. and Brady, J.M. (1997), "SUSAN – a new approach to low level image processing", *International Journal of Computer Vision*, Vol. 23 No. 1, pp. 45-78, doi: 10.1023/A:1007963824710.

Sundla, S., Punning, A., Aabloo, A. and Anbarjafari, G. (2015), "Semi-automatic deflection measurement using digital image correlation", *19th International Conference on System Theory, Control and Computing, ICSTCC 2015 – Joint Conference SINTES 19, SACCS 15, SIMSIS 19*, pp. 325-330, doi: 10.1109/ICSTCC.2015.7321314.

Torr, P.H.S. and Zisserman, A. (2000), "MLESAC: a new robust estimator with application to estimating image geometry", *Computer Vision and Image Understanding*, Vol. 78 No. 1, pp. 138-156, doi: 10.1006/CVIU.1999.0832.

Tsvetkov, R., Shardakov, I., Shestakov, A., Gusev, G. and Epin, V. (2017), "Deformation monitoring of load-bearing reinforced concrete beams", *Procedia Structural*

Integrity, Vol. 5, pp. 620-626, doi: 10.1016/j.prostr.2017.07.028.

Tuytelaars, T. and Mikolajczyk, K. (2008), "Local invariant feature detectors: a survey", *Foundations and Trends® in Computer Graphics and Vision*, Vol. 3 No. 3, pp. 177-280, doi: 10.1561/0600000017.

Tuytelaars, T. and Van Gool, L. (1999), "Content-based image retrieval based on local affinely invariant regions", in Huijsmans, D.P. and Smeulders, A.W.M. (Eds), *Visual Information and Information Systems*, Springer Berlin Heidelberg, pp. 493-500.

Tuytelaars, T. and Van Gool, L. (2000), "Wide baseline stereo matching based on local, affinely invariant regions", *British Machine Vision Conference*, pp. 412-425.

Tuytelaars, T. and Van Gool, L. (2004), "Matching widely separated views based on affine invariant regions", *International Journal of Computer Vision*, Vol. 59 No. 1, pp. 61-85, doi: 10.1023/B:VISI.0000020671.28016.e8.

Valença, J. and Júlio, E.S. (2017), "Vision-SHM method for structural monitoring based on photogrammetric computer vision", *IABSE Conference, Bath 2017: Creativity and Collaboration - Report*, Vol. 108 No. 1, pp. 366-373, doi: 10.1016/j.biomaterials.2014.08.012.

Xiao, Z., Liang, J., Yu, D. and Liu, J. (2010), "Rapid three-dimension optical deformation measurement for transmission tower with different loads", *Optics and Lasers in Engineering*, Vol. 48 No. 9, pp. 869-876, doi: 10.1016/J.OPTLASENG.2010.04.003.

Zhao, W., Yan, L. and Zhang, Y. (2018), "Geometric-constrained multi-view image matching method based on semi-global optimization", *Geo-Spatial Information Science*, Vol. 21 No. 2, pp. 115-126, doi: 10.1080/10095020.2018.1441754.

Corresponding author

Farid Esmaeili can be contacted at: farid_63@yahoo.com